# Optimization of Dimpled Surface of NACA0012 Airfoil to Enhance the Aerodynamic Performance

Olajide Sulaiman Olayiwola<sup>1</sup>, Mahadi Hasan Masud<sup>2</sup>, Abu Kaisar Md Faisal<sup>3</sup>, Milind Siddhpura<sup>4</sup>, Arti Siddhpura<sup>5</sup>

<sup>1, 4, 5</sup>Engineering Institute of Technology (EIT), Australia

<sup>2</sup> Engineering Institute of Technology (EIT), Australia, Department of Mechanical Engineering, Rajshahi University of Engineering & Technology, Rajshahi-6204, Bangladesh

<sup>3</sup> Department of Mechanical Engineering, Rajshahi University of Engineering & Technology, Rajshahi-6204, Bangladesh

Abstract:-This study investigates the impact of dimple surfaces on the aerodynamic performance of NACA0012 airfoil. Numerical analyses were conducted to compare the aerodynamic performance of baseline, dimples, and optimized airfoil. Two-dimensional simulations of the airfoil were undertaken to investigate superior dimple configuration between inward and outward dimples, optimum dimple diameter, and optimum dimple position relative to the chord length. The simulation was conducted using Ansys fluent, employing the steady SST k-ω turbulence model with a fluid velocity of 18 m/s (chord-based Reynolds number of 6.7 \* 10<sup>4</sup>). The result of the study shows that inward dimples located at different positions on the upper surface of the airfoil at 8-degree angle of attack have superior aerodynamic performance in terms of lift-to-drag (LtD) ratio. Numerical simulations were conducted for nine distinct Minitab optimization design cases for dimpled NACA0012 airfoil to identify and validate optimum dimple diameter and dimple position relative to the chord length of the airfoil. Concerning the NACA0012 chord, the optimum dimple diameter is 2 mm, and the optimum dimple position is 47.26% for the airfoil's leading edge. Dimple surface optimization also brings about delayed boundary layer separation, reduction in drag coefficient, and, consequently, increases the LtD ratio.

Keywords: Aerodynamic Efficiency, Dimple Surface, Low-Reynolds Number, Optimization.

#### 1. Introduction

National Advisory Committee for Aeronautics (NACA) airfoils are most commonly used for wind turbine blades, aircraft wings, rotor blades, and propellers, but they have efficiency and stall angle difficulties. To tackle engineering problems in seemingly distinct industries, researchers always explore nature and existing technology in other domains or industries to overcome stall angle and efficiency. Based on the dimpled surface of a gulf ball, dimple application on airfoil surfaces has shown promising results, making it an emotive topic among aerospace and CFD engineering researchers and industrial specialists. This study aims to optimize the dimpled surface of the NACA0012 airfoil to improve its aerodynamic efficiency. A NACA0012 airfoil's maximum thickness is 12% of its chord length. Fig. 1 shows the basic terminology of an airfoil.

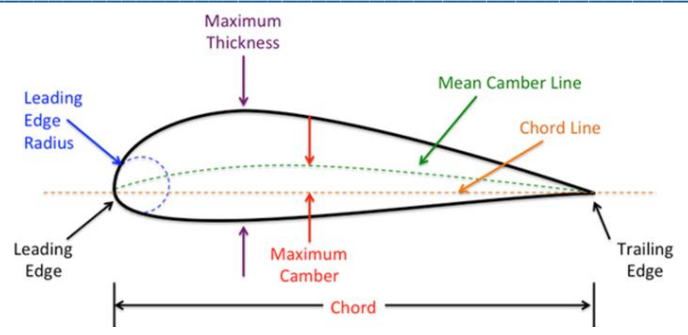


Fig. 1: Basic airfoil terminologies

Several studies highlight the significant impact of dimples on airfoil performance, particularly in delaying boundary layer separation, reducing drag, and enhancing lift across different angles of attack (AoA) [1]–[4]. Vandrangi (2022) [5]emphasizes the importance of airfoil selection for wind turbine efficiency, while Srivastav (2012) [6] and Kaushik *et al.* (2018) [7] demonstrate that outward and inward dimples improve lift-to-drag (LtD) ratios, especially at higher AoA. Chear and Dol (2015) [8] and Hasen *et al.* (2020) [9] found that dimples generate turbulence, which delays flow separation and reduces drag. Saraf *et al.* (2015, 2017) [10], [11] and Devi *et al.* (2020) [12] further support the effectiveness of dimples, noting optimal dimple locations and shapes for maximum aerodynamic efficiency. Hossain *et al.* (2015) [13] and Mustak *et al.* (2017) [14] confirm that dimples delay stall, increasing lift and extending the operational AoA range, while Biradar *et al.* (2017) [15] show that dimples reduce drag regardless of their configuration. Overall, dimples significantly improve the aerodynamic characteristics of airfoils, offering the potential for enhanced performance in various applications. Moreover, dimples delay boundary layer separation and reduce wake production, improving airfoil aerodynamic efficiency. It enhances lift force, reduces drag at positive AoA, and raises stall angle. Future research could optimize the dimple dimension relative to chord length, the number of dimples per airfoil, inter-dimple spacing, dimple position from the leading edge, and AoA.

A thorough literature study found that dimple application improves airfoil aerodynamic efficiency without dimple parameter adjustment. One can only imagine how optimization can improve airfoil performance and efficiency. Since more needs to be done to optimize NACA0012 airfoil dimple surfaces, this study optimizes semicircular dimple diameter and dimple position with respect to the leading edge.

#### 2. Methodology and Modeling

## A. Methodology

Submit Using a numerical method (Ansys Fluent simulation) with a consistent fluid domain, Reynolds number (Re), and varying angle of attack (AoA), baseline and dimpled NACA0012 airfoils were compared for LtD ratio. The dimpled surface was then optimized. Figure 2 summarizes an overview of the methodology implemented in the current study.



Fig. 2: Summary of research methodology

#### B. Theories

It is generally accepted that the application of dimples on airfoil surfaces results in improved aerodynamic performance. Still, different authors differ in their view of which geometry, configuration (inward or outward), and dimple position works best in terms of aerodynamic efficiency. One of these research studies aims to improve the  $C_L/C_D$  ratio, not only to improve  $C_L$  But also to minimize  $C_D$ . Aerodynamic performance coefficients can be expressed analytically, as shown in equations 1 and 2.

$$C_L = \frac{2F_l}{\rho S u^2} \tag{1}$$

$$C_D = \frac{2F_d}{\rho S u^2} \tag{2}$$

$$\frac{C_L}{C_D} = \frac{F_l}{F_d} \tag{3}$$

$$Re = \frac{\rho uL}{\mu} = \frac{uL}{\nu} \tag{4}$$

Where,  $F_l$  is aerodynamic lift force,  $F_d$  is aerodynamic drag force,  $\rho$  is air density, S is wing area, u is speed, and  $\mu$  is viscosity.

Eq. 4 depicts the Reynolds number Re, which is a dimensionless quantity determining laminar, transitional, or turbulent flow [16], [17]. In the equation,  $\rho$  represents air density, L represents characteristic length,  $\mu$  represents dynamic viscosity, and  $\nu$  represents kinematic viscosity.

## C. Turbulence Modeling

Numerically solving Navier-Stokes equations is expensive and time-consuming. Turbulence models like the k-ε turbulent model and the k-\omega turbulent solve the problem; they are widely used in the case of analyzing both bluff and streamlined bodies [10]. SST (Shear Stress Transport) k-ω turbulence model is a popular two-equation eddy-viscosity model. This model can be used as a Low-Re turbulence model without damping functions, as it uses a k-ω formulation in the inner boundary layer and can be applied directly to the wall via the viscous sublayer. The SST formulation solves the k-ω model's sensitivity to inlet free-stream turbulence factors by adopting a k-ε behavior in the free-stream. The SST k-ω model is often praised for its performance in challenging pressure gradients and separating flow [11]. The SST k-ω turbulence model, widely accepted in both the industrial and educational sectors was chosen for this study due to its more accurate prediction of flow separation compared to most RANS models, leading to its superior performance under unfavorable pressure gradients. The turbulence kinetic energy (k) is the first variable in the model, and the specific rate of dissipation (of the turbulence kinetic energy k into internal thermal energy) is the second variable ( $\omega$ ). The model uses two partial differential equations to try and forecast turbulence. The k- ω turbulent model is represented in equations 6 and 7. Masud et al. (2024), Masud and Dabnichki (2023), Devi (2020), and Saraf et al. (2017) are some of the previous researchers who have used the DES SST k- ω turbulent model for airfoil simulation in Ansys fluent [11], [12], [16], [18].

$$V_T = \frac{k}{\omega} \tag{5}$$

$$\frac{\partial}{\partial t}(\rho k) + \frac{\partial}{\partial x_i}(\rho u_j k) = \rho P - \beta^* \rho \omega k + \frac{\partial}{\partial x_i} \left[ \left( \mu + \sigma_k \frac{\rho k}{\omega} \right) \frac{\partial k}{\partial x_i} \right]$$
 (6)

$$\frac{\partial}{\partial t}(\rho\omega) + \frac{\partial}{\partial x_{i}}(\rho u_{j}\omega) = \frac{\alpha\omega}{k}\rho P - \beta\rho\omega^{2} + \frac{\partial}{\partial x_{i}}\left[\left(\mu + \sigma_{\omega}\frac{\rho k}{\omega}\right)\frac{\partial\omega}{\partial x_{i}}\right] + \frac{\rho\sigma_{d}}{\omega}\frac{\partial k}{\partial x_{i}}\frac{\partial\omega}{\partial x_{i}}$$
(7)

$$P = \tau_{ij} \frac{\partial u_i}{\partial x_j} \tag{8}$$

#### D. Geometry

NACA0012 airfoil coordinate points with a 55mm chord were obtained from the Airfoil Tools database. The coordinate points were imported into SolidWorks CAD software to generate the NACA0012 airfoil model (see Fig. 3). Dimples of different diameters and positions from the leading edge were also introduced on the airfoil surface using SolidWorks.

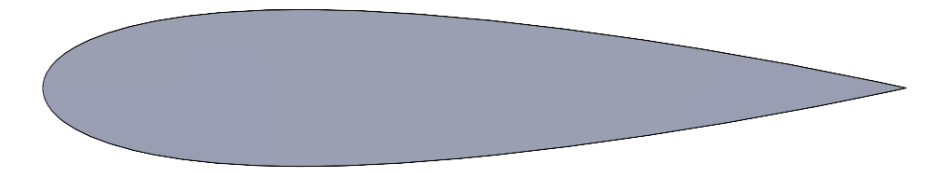


Fig. 3: NACA0012 geometry of 55 mm chord

#### E. Domain setup

After importing the 2D NACA0012 model from SolidWorks with a chord length of 55mm, the computational fluid domain dimension was set to around 1000% of the NACA0012 airfoil's chord length (see Fig. 4). For good meshing, the fluid domain is separated into four bodies with dimensions of 1650 mm \* 600 mm, 1450 mm \* 400 mm, 1250 mm \* 200 mm, and 1050 mm \* 100 mm. The  $Y^+$  value was set to 1, and the first layer thickness is  $1.5*10^{-5}$  m to attain that specific  $Y^+$  (see Fig. 5 for details).

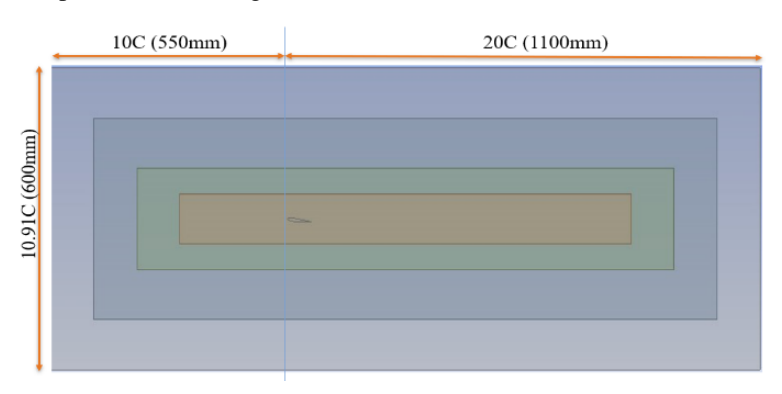


Fig 4: Geometry of the airfoil and the fluid domain setup

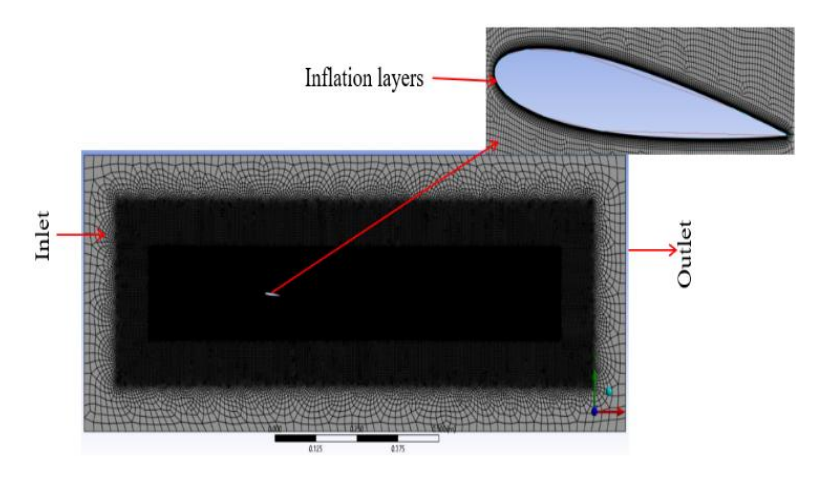


Fig 5: Generated mesh for the current study

#### F. Mesh Sensitivity Analysis

To achieve reliable, repeatable, and dependable results, mesh sensitivity analysis was performed at all the AoA; however, results for only  $6^{\circ}$  AoA is shown in Table I. The mesh sensitivity analysis was performed by gradually increasing the number of elements by lowering body and edge size until a good-quality fine mesh was attained. The evaluation parameters, i.e., lift and drag coefficients did not change while performing the numerical analysis. Through mesh sensitivity analysis, maximum skewness and orthogonal quality were kept within the acceptable limits. As highlighted in Table I and Fig. 6, number of elements = 433,307 were used with a maximum skewness of 0.826330 and orthogonal quality of 1.0, which are in the acceptable range.

Number of Elements	Max Skewness	Max Orthogonal Quality	$C_L$	$C_D$
8019	0.99998	1.0	0.65016577	0.038235491
27436	0.99995	1.0	0.53438856	0.032777750
36822	0.99994	1.0	0.52596038	0.031979585
51600	0.99992	1.0	0.51122177	0.031123111
71798	0.99990	1.0	0.51324676	0.031149778
102779	0.99987	1.0	0.52673863	0.030000758
125854	0.83023	1.0	0.48333286	0.027941483
154834	0.82957	1.0	0.49731304	0.027165706
189329	0.82897	1.0	0.51246369	0.026411655
234287	0.82858	1.0	0.53185432	0.025702578
287062	0.82836	1.0	0.53552151	0.025086339
353726	0.82544	1.0	0.54153516	0.024718975
391143	0.838530	1.0	0.54545141	0.024523713
433307	0.826330	1.0	0.55066107	0.024184598
479254	0.828190	1.0	0.55066107	0.024184598
498588	0.827430	1.0	0.55066107	0.024184598

Table I. Mesh Sensitivity Analysis Value at 6°AoA

## G. Numerical Boundary & Simulation setup

Ansys FLUENT 2023 (Student version) was used to do the flow simulations. The steady Reynolds-averaged Navier-Stokes (RANS) model, i.e., the shear stress transport (SST) k-  $\omega$  turbulence model was used for the current study. The AoA was varied from 0 to 20 degrees with an interval of 2 degrees for baseline airfoil and inward and outward dimpled airfoil. With the airfoil chord of 55mm, the free stream velocity was 18m/s, and the Reynolds number was set at 67000. Tables II and III demonstrate the simulation reference values and setup parameters.

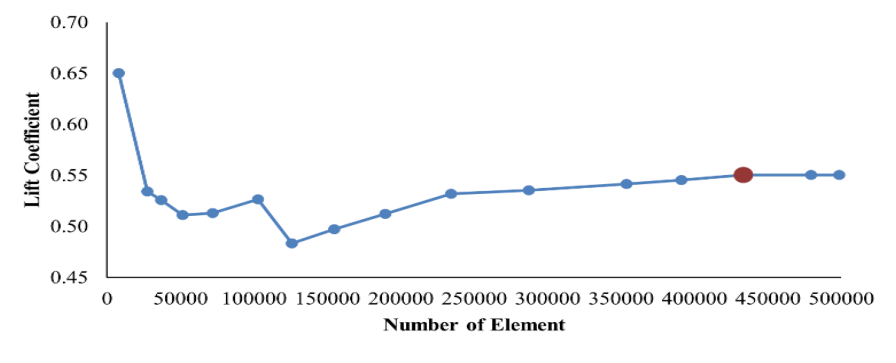


Fig 6: Mesh sensitivity analysis plot at 6 ° AoA.

**Table III. Simulation Reference Values** 

Parameter	Туре
Chord, C	0.055m
Area, A	$0.055 \text{m}^2$
Density	1.225 kg/m <sup>3</sup>
Characteristic Length	0.055m
Velocity	18 m/s
Dynamic Viscosity	1.7894*10 <sup>-5</sup> kg/(ms)
Reynolds Number	67000

**Table IIIII. Simulation Setup Parameter** 

Parameter	Туре	
Airfoil Type	NACA0012	
Solver	Pressure-Based	
Analysis Type	Steady-state	
Reynolds Number	67,000	
Simulation configuration	2D	
Turbulence Model	Standard k-ω SST	
Inlet	Velocity-Inlet	
Outlet	Pressure-Outlet	
Airfoil Wall	No-slip, Wall	
Compute region	Inlet	
Material	Air	
Reported Definition	Lift coefficient	
Reported Definition	Drag coefficient	

# H. Dimple position and diameter optimization

The current study aims to optimize the dimple diameter and position on the NACA0012 airfoil for  $8^{\circ}$  AoA. A Preliminary optimization was conducted using semicircular inward and outward dimples to establish the range for optimization. The dimple diameter and depth were set at 3.2% and 1.6% of the chord, and various dimple positions relative to the LE were considered, as shown in Table IV. This preliminary study will determine the optimal dimple position and configuration for improved aerodynamic performance in terms of lift coefficient  $(C_L)$ , drag coefficient  $(C_D)$ , and LtD ratio.

Table IV. Inward and outward airfoil geometry design

DimplePositionfro m LE	Inward Dimple	Outward Dimple
10%		
20%		
40%		

DimplePositionfro m LE	Inward Dimple	Outward Dimple
60%		
80%		

## I. Minitab model generation parameter for optimization

Table V shows Minitab's 13 design instances at 8° AoA, based on upper and lower bound dimple diameter and position, from the preliminary optimization procedure. These designs were considered for both inward and outward dimples. One design example (Design F) was reproduced five times, creating nine scenarios. The design samples were modeled in SolidWorks and loaded into the Ansys design modeler to ensure fluid domain and reference parameters based on the baseline airfoil.

**Position from** Position form StdOrder/ Blocks/PtType Design Diameter (mm) LE (%) LE (mm) RunOrder Α 10 5.5 1 1 1 В 2 45.335 2 82.43 1 3.414  $\mathbf{C}$ 40 22 3 1 D 1 **70** 38.5 4 1 5 E 2 5.5 1 10 F 2 40 22 6 1 F 2 40 22 7 1 G 3 8 1 **70** 38.5 F 9 2 22 1 40 Η 3 10 5.5 10 1 F 2 40 22 11 1 I 0.586 40 12 1 22 F 2 40 22 13 1

Table V. Minitab Optimization Design parameters at 8° AoA

#### 3. Result And Discussion

#### A. Validation of Simulation Setup

Numerical analysis on the baseline NACA0012 airfoil was performed and validated by comparing the results to Yasuda *et al.* [REF]. The setup parameters were set identically to those of the Yasuda *et al.* (2019) [19] paper to run the simulation and validate the results. Compared to the results reported by Yasuda *et al.* (2019), the numerical results obtained in the current study are almost similar (see Fig. 7 for details).

#### B. Dimple type selection: inward or outward

Numerical analysis was conducted to obtain the result of preliminary optimization for inward and outward dimples and the approximate dimple position relative to LE. Figure 8 illustrates the comparison of aerodynamic performance for inward and outward dimples against their relative position to the LE. The investigation of dimple configurations and positions shows that the inward dimple configuration has superior aerodynamic performance against the outward dimple, which can be seen in Fig. 8 (a), (b), and (c). A dimple position between 40% and 60% shows improved lift coefficient and LtD and decreased drag coefficient. Hence, an

inward dimple was selected for the Minitab optimization, and the lower and upper bounds were given based on these results. Fig. 9 shows the designs suggested by Minitab, where an inward dimple was selected.

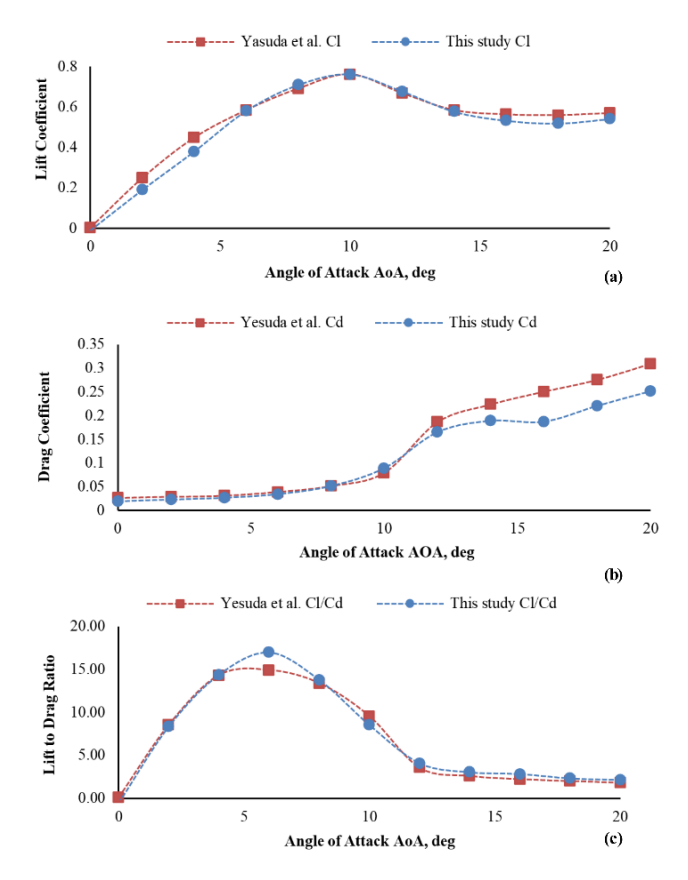


Fig 7: Validation of the simulation result with published research [13].

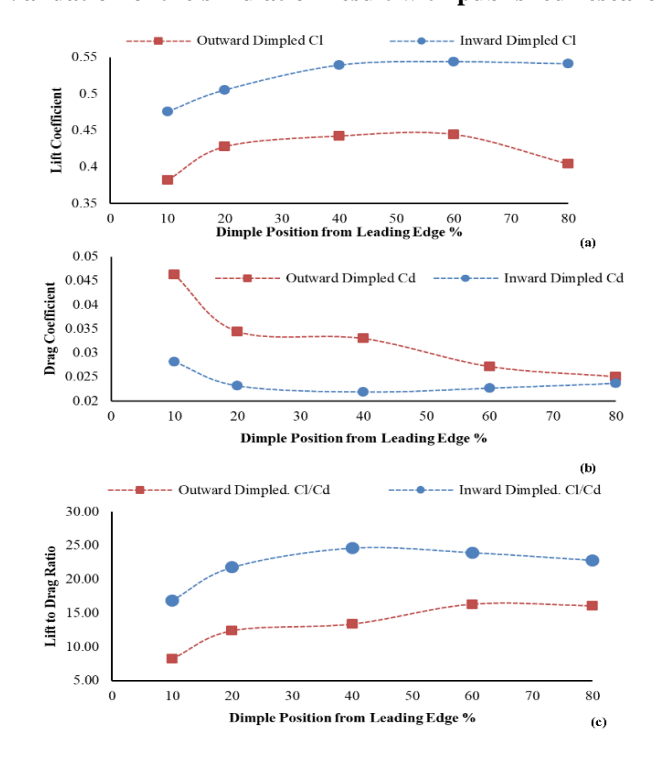


Fig 8: Inward and outward dimple (a)  $C_L$ , (b)  $C_D$ , and (c)  $C_L/C_D$  vs Position from LE at  $6^{\circ}AoA$  plots

Design A

Design E

Design B

Design C

Design G

Design II

Fig 9: 2D Airfoil configuration models based on Minitab design parameters.

## C. Dimple optimization

Minitab designs were simulated in Ansys Fluent at the same condition as the baseline airfoil at an  $8^{\circ}$  AoA. The LtD ratios were computed for each design and analyzed in Minitab, with dimple diameter and position as continuous factors and LtD ratio as the response factor (see Table VI for details).

Design	Diameter (mm)	Position fromLE (%)	C <sub>L</sub> /C <sub>D</sub>
A	1	10	18.713458
В	2	82.43	24.011679
С	3.414	40	27.084217
D	1	70	23.362484
Е	2	10	16.604789
F	2	40	26.184547
F	2	40	26.184547
G	3	70	24.441773
F	2	40	26.184547
Н	3	10	11.341285
F	2	40	26.184547
I	0.586	40	23.59642
F	2	40	26.184547

Table VI. Minitab Optimization Design's C<sub>I</sub>/C<sub>D</sub> at 8° AoA

# D. 2D Contour Plot and 3D Surface plot

Figs. 10 (a) and (b) show dimple position (% LE), diameter, and LtD ratio. The dimple diameter and position are inputs. Adjusting input factors improves output, especially the LtD ratio. Dimples should be greater than 1.6 mm and located between 45% and 68%. At that position, the ideal lift-to-drag ratio exceeds 27.

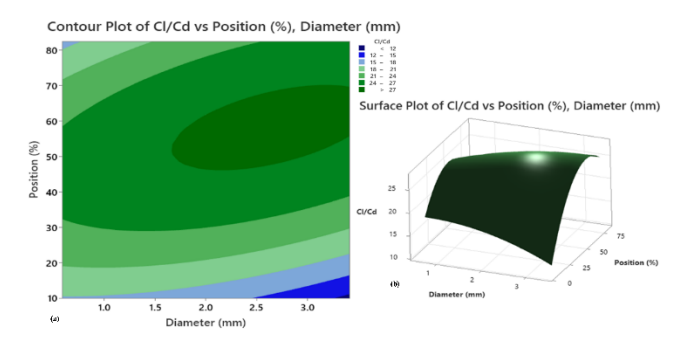


Fig 10: Minitab (a) Contour plot, and (b) Surface plot of C<sub>L</sub>/C<sub>D</sub> vs dimple position and diameter.

## E. Response Optimization

Response Surface Methodology (RSM) was utilized in Minitab to optimize the dimple diameter and position. Minitab's response optimizer predicts the best factor combination for the response variable shown in Fig. 11. Minitab predictions were validated with Ansys fluent; hence, the project employed a targeted response. Ansys simulations mirrored Minitab predictions, especially at the maximum response setting. The Minitab program estimates the appropriate dimple size and location on a 55 mm-chord NACA0012 airfoil. The ideal dimple diameter is 2 mm, and the position is 47.26% of the chord length from the leading edge. As seen in Fig. 11, Minitab estimates  $C_L/C_D$  at 27.08. By using SolidWorks, optimized 2D model of NACA0012 with a 55mm chord length and a Minitab-recommended dimple diameter and position was generated. The predicted results of Minitab's  $C_L/C_D$  were confirmed by simulation.

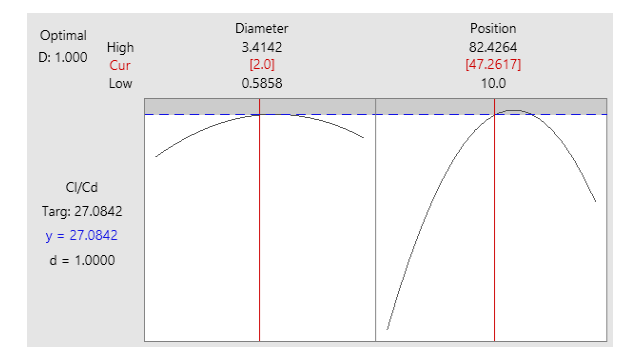


Fig 11: Minitab Response surface optimizer plot.

## F. Aerodynamic Performance of Optimized Airfoil

Fig. 12 illustrates the aerodynamic performance comparison between baseline, inward dimple, and outward dimple airfoils across a range of angles of attack (AoA) from 6° to 16°.

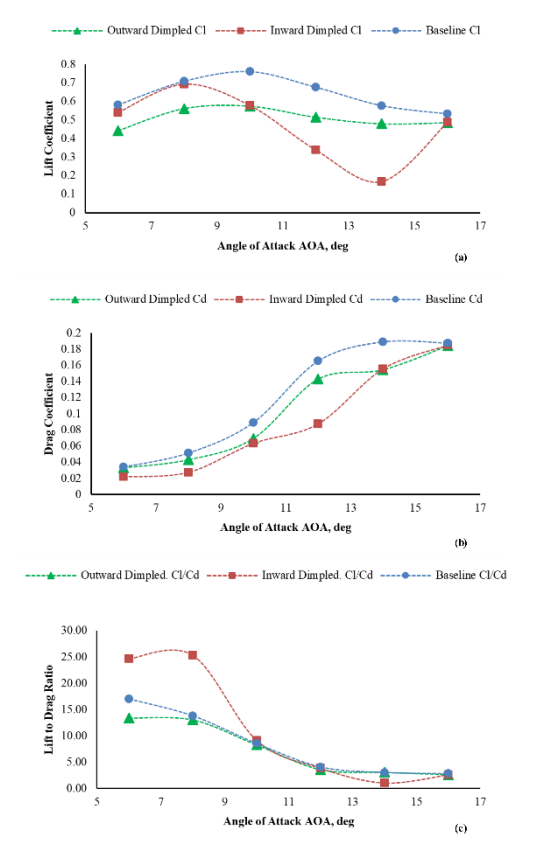


Fig 12: Inward dimple, outward dimple, and baseline (a) C<sub>L</sub>, (b) C<sub>D</sub>, and (c) C<sub>L</sub>/C<sub>D</sub> vs AoA

In Fig. 12 (a), it is evident that at AoA of 6-8°, the lift performance of the inward dimple airfoil is similar to that of the baseline airfoil. However, beyond 8° AoA, the lift decreases until 16°, which becomes identical to the baseline. On the other hand, the outward dimple airfoil consistently exhibits lower lift performance across all AoA ranges. Moving on to Fig. 12 (b), which reveals the drag coefficients for the three airfoils across the AoA range. It is clear that the inward dimple airfoil has the lowest drag coefficient among all three airfoils. At 16° AoA, its drag coefficient becomes similar to the baseline. Interestingly, in terms of drag generation, the outward dimple airfoil also performs better than the baseline. Finally, Fig. 12 (c) shows that at 8° AoA, the inward dimple airfoil has the highest lift-to-drag ratio among the three airfoils. However, this value gradually decreases as AoA increases. The aerodynamic performance of the optimized dimple surface of the NACA0012 airfoil was systematically evaluated under the same conditions as the baseline at 8° AoA, ensuring reliable data and results in comparison. Table VII compares the optimal and baseline airfoil's aerodynamic performance. The optimized airfoil has a higher LtD ratio than the baseline aerofoil.

Table VII. Minitab Optimization Design parameters at 8° AoA

Design	Diameter (mm)	Position fromLE(%)	$C_{L}$	C <sub>D</sub>	C <sub>L</sub> /C <sub>D</sub>
Baseline	-	-	0.709	0.0514	13.792
Optimization	2	47.2617	0.692	0.0253	27.316

#### G. Pressure Coefficient

Fig. 13 shows pressure coefficient ( $C_p$ ) plots as the fluid passes across the baseline NACA0012 and optimized airfoil at 8° AoA. The airfoil pressure coefficient is the ratio of pressure force to internal force. Lift force is generated by increased pressure on the lower surface of the airfoil and decreased pressure at the upper surface of the airfoil. As shown in the pressure coefficient figure, the baseline and optimized airfoil have the same trend; hence, optimizing the dimpled surface has little effect on the pressure coefficient data, which can also be seen from the lift coefficient values shown in Table VII.

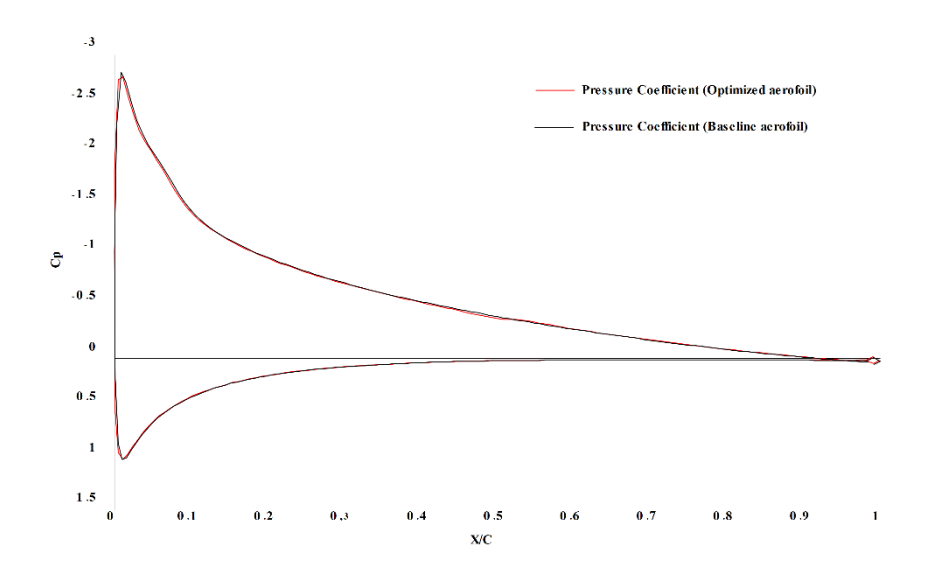


Fig 13: Pressure Coefficient plot for Baseline and Optimized airfoil at 8°AoA.

## H. Pressure Contour Plot

Fig. 14 illustrates pressure contour plots indicating that the pressure distribution around the optimized NACA0012 surface and the baseline is almost indistinguishable. This suggests that at an 8° angle of attack, the pressure concentration around the airfoil remains unaffected by the use or optimization of dimples.

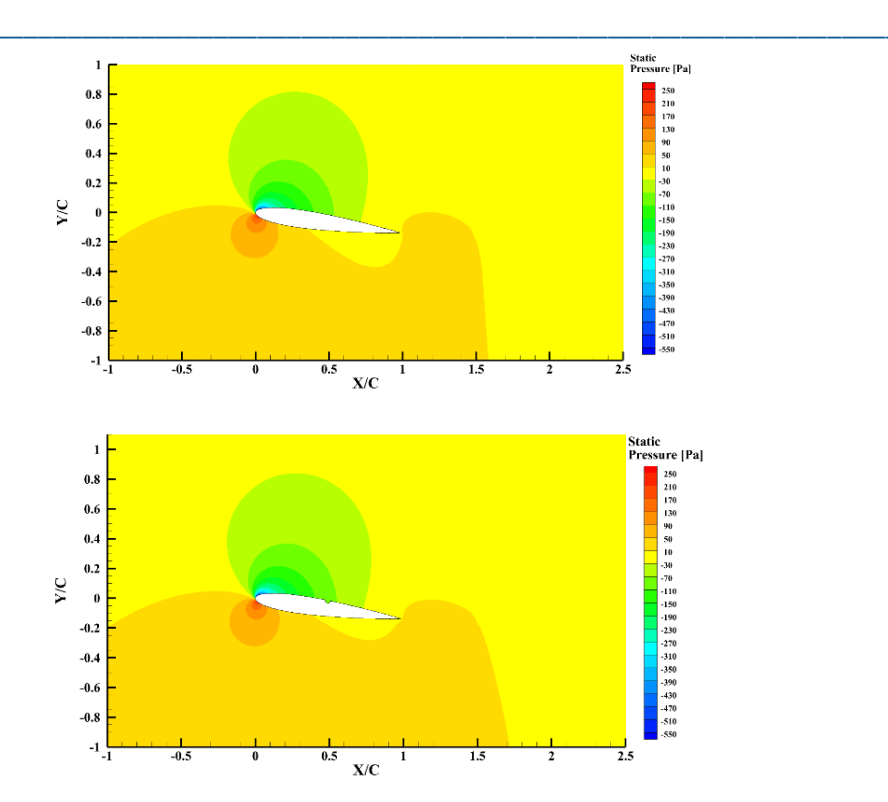


Fig 14: Pressure contour for Baseline (Top) and Optimized (Bottom) NACA0012 airfoil at 8°AoA.

## I. Velocity Streamlines

In Figure 15, the velocity streamlines are depicted for both the baseline and optimized NACA0012 airfoils at an angle of attack (AoA) of 8 degrees. It is observed that there is no significant change in the boundary layer separation between the two airfoils.

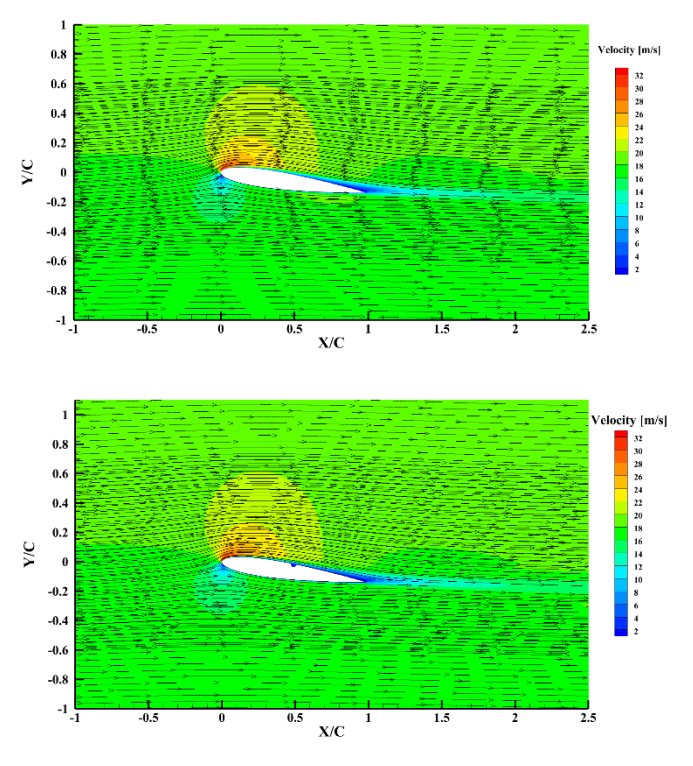


Fig 15: Velocity streamline for baseline (Top) and Optimized (Bottom) airfoil at 8°AoA.

#### 4. Conclusion

This study examines the numerical simulation of plain, dimpled, and optimized NACA0012 airfoils, specifically focusing on dimple optimization and its impact on aerodynamic performance. Nine Minitab design cases were simulated in Ansys Fluent to calculate lift-to-drag ratios, which were then used in Minitab to predict optimal dimple parameters. The optimal dimple diameter was 2mm, positioned 47.27% from the leading edge, yielding a lift-to-drag ratio of 27.08. Validation through Ansys Fluent confirmed a similar ratio of 27.32.

The study underscores the significance of the findings that random dimple application does not guarantee improved performance; therefore, dimple shape, size, position, and configuration optimization are crucial. Evaluating aerodynamic performance using the lift-to-drag ratio offers a more balanced assessment than isolated lift or drag coefficients. As revealed in this study, the results demonstrate that dimple optimization significantly improves aerodynamic performance by enhancing the LtD ratio, delaying boundary layer separation, and reducing drag compared to the baseline airfoil.

#### References

- [1]. S. S. Mahamuni, "A Review on Study of Aerodynamic Characteristics of Dimple Effect on Wing," International Journal of Aerospace and Mechanical Engineering, vol. 2, no. 4, 2015.
- [2]. M. T. Islam, A. M. E. Arefin, M. H. Masud and M. Mourshed, "The effect of Reynolds number on the performance of a modified NACA 2412 airfoil," p. 2018.
- [3]. M. H. Masud, Naim-Ul-Hasan, A. M. E. Arefin and M. U. H. Joardder, "Design modification of airfoil by integrating sinusoidal leading edge and dimpled surface," 2017.
- [4]. B. K. Sreejith and A. Sathyabhama, "Experimental and numerical study of laminar separation bubble formation on low Reynolds number airfoil with leading-edge tubercles," Journal of the Brazilian Society of Mechanical Sciences and Engineering, vol. 42, no. 4, p. 171, Apr 2020.
- [5]. D. B. Srivastav, "Flow Control over Airfoils using Different Shaped Dimples".
- [6]. S. K. Vandrangi, "Aerodynamic characteristics of NACA 0012 airfoil by CFD analysis," Journal of Airline Operations and Aviation Management, vol. 1, no. 1, 2022.
- [7]. V. Kaushik, M. Mahore and S. Patil, "Analysis of dimpled wing of an aircraft," International Journal of Engineering Development and Research, 2018.
- [8]. C. K. Chear and S. S. Dol, "Vehicle Aerodynamics: Drag Reduction by Surface Dimples".
- [9]. D. Hasen, S. Elangovan, M. Sundararaj and K. M. Parammasivam, "CFD Analysis of Controlling the Airflow over Airfoils using Dimples: Technical Note," International Journal of Vehicle Structures and Systems, vol. 11, no. 5, 2020.
- [10]. K. Saraf, M. P. Singh and T. S. Chouhan, "Effect of Dimple on Aerodynamic Behaviour of Airfoil".
- [11]. K. Saraf, M. P. Singh and T. S. Chouhan, "Aerodynamic analysis of NACA0012 airfoil using CFD," 2017.
- [12]. P. B. Devi, R. Gokulnath, D. R. Joseph and V. Paulson, "Aerodynamic Behaviour of Dimpled NACA0012 Airfoil for Various Angles of Attack: Technical Note," International Journal of Vehicle Structures and Systems, vol. 11, no. 4, Jan 2020.
- [13]. M. Hossain, N. M. Uddin, R. Mustak and M. Mashud, "Experimental study of aerodynamic characteristics of airfoils using different shaped dimples," International Journal Of Engineering And Science (IJES), 2015.
- [14]. R. Mustak and R. Molla, "Improvement of Aerodynamic Characteristics of an Airfoil by Surface Modification," American Journal of Engineering Research (AJER), no. 6, p. 7–14, 2017.
- [15]. S. Biradar, "CFD Analysis of Dimple Effect on Airfoil Naca 0015," Int J Res Appl Sci Eng Technol, vol. V, no. IX, p. 369–374, Sep 2017.
- [16]. M. H. Masud and P. Dabnichki, "Feasibility of penguin geometric features for the biomimetics applications: overview and analysis," Meccanica, vol. 58, no. 5, p. 847–858, May 2023.
- [17]. T. Yasuda, K. Fukui, K. Matsuo, H. Minagawa and R. Kurimoto, "Effect of the Reynolds Number on the Performance of a NACA0012 Wing with Leading Edge Protuberance at Low Reynolds Numbers," Flow Turbul Combust, vol. 102, no. 2, p. 435–455, Feb 2019.

Tuijin Jishu/Journal of Propulsion Technology

ISSN: 1001-4055 Vol. 45 No. 3 (2024)

[18]. M. H. M. a. P. Dabnichki, "Aerodynamic Performance Analysis of Penguin-Inspired Biomimetic Aircraft Wing," Green Approaches in Sustainable Aviation, Springer, pp. 115-120, 2024.

[19]. M. H. Masud and P. Dabnichki, "Strouhal number analysis for the swimming of little penguin (Eudyptula minor): Proof of efficient underwater propulsion," Results in Engineering, vol. 17, p. 100840, Mar 2023.